PROCEEDINGS A

royalsocietypublishing.org/journal/rspa

Research

Cite this article: Ghanbarzadeh A, Faraji M, Neville A. 2020 Deterministic normal contact of rough surfaces with adhesion using a surface integral method. *Proc. R. Soc. A* **476**: 20200281. http://dx.doi.org/10.1098/rspa.2020.0281

Received: 22 April 2020
Accepted: 4 September 2020

Subject Areas:
mechanical engineering, materials science, mechanics

Keywords:
contact mechanics, roughness, adhesion, Lennard-Jones potential

Author for correspondence:
Ali Ghanbarzadeh
e-mail: a.ghanbarzadeh@leeds.ac.uk

Deterministic normal contact of rough surfaces with adhesion using a surface integral method

Ali Ghanbarzadeh[1], Mostafa Faraji[2] and Anne Neville[1]

[1]Institute of Functional Surface, School of Mechanical Engineering, University of Leeds, Leeds, LS2 9JT, UK
[2]Institute for Computational Mechanics, Technische Universität München, Boltzmannstr. 15, 85747 Garching b. München, Germany

AG, 0000-0002-3815-2523

The fundamental problem of adhesion in the presence of surface roughness and its effect on the prediction of friction has been a hot topic for decades in numerous areas of science and engineering, attracting even more attention in recent years in areas such as geotechnics and tectonics, nanotechnology, high-value manufacturing and biomechanics. In this paper a new model for deterministic calculation of the contact mechanics for rough surfaces in the presence of adhesion is presented. The contact solver is an in-house boundary element method that incorporates fast Fourier transform for numerical efficiency. The adhesive contact model considers full Lennard-Jones potentials and surface integration at the asperity level and is validated against models in the literature. Finally, the effect of surface roughness on the adhesion between surfaces was studied, and it was shown that the root mean square gradient of surface roughness can change the adhesive pressures irrespective of the root mean square surface roughness. We have tested two adhesion parameters based on Johnson's modified criteria and Ciavarella's model. We showed that Civarella's model introduces the most reasonable criteria suggesting that the RMS roughness and large wavelength of surfaces roughness are the important parameters of adhesion between rough surfaces.

1. Introduction

Adhesion is the term used when two surfaces are attracted to each other due to different forces such

THE ROYAL SOCIETY PUBLISHING

as inter-atomic Van Der Waals forces, electrostatic and capillary forces. The magnitude of this force is often correlated to the nature of the molecules and the distance of separation between them [1]. Often in engineering, in particular solid mechanics, adhesion is referred to as the attractive forces between non-bonding atoms or molecules of surfaces and the Lennard-Jones is often used as a model potential providing a qualitative description of intermolecular forces to describe the attraction/repulsion as a function of their separation. When two real engineering bodies come into contact, there will be areas of surfaces which are in physical contact and the contact pressure is compressive. Depending on the topography of the surfaces, there will be a distribution of surface separations across the nominal contact area. These separations, if small enough (with respect to atomic distances), can lead to attractive forces between surface points.

In contact mechanics, there are numerous models of adhesive contact [2]. In particular, there are two widely used analytical adhesive models both developed for smooth surfaces, namely, Johnson–Kendall–Roberts (JKR) [3] and Derjaguin–Muller–Toporov (DMT) [4]. In JKR, it is assumed that there is no adhesion outside the contact area and infinitely large pressures are present at the border and inside the contact area. By contrast, DMT assumes a Hertzian contact area with consideration of adhesion and adhesion forces do not contribute to surface deformations. Both models have their limitations in the application, which makes JKR valid for the case of soft materials and large radius of curvature and DMT valid for stiffer materials with small curvatures. There is a wealth of engineering problems that would sit outside these constraints and also a high proportion of engineering contact problems involves rough surfaces. David Tabor showed that the validity of the JKR and DMT models can be assessed by the Tabor parameter (μ) [5] where JKR can effectively predict adhesion at large values of (μ) and DMT at smaller values. Maugis [6] developed a model based on the Dugdale approximation using Lennard-Jones potentials and bridged the transition gap between DMT and JKR which, to date, remains a more complete description of the adhesive contact model for smooth surfaces. Muller *et al*. [7] and later Greenwood [8] developed a complete numerical solution for the contact with adhesion by applying Lennard-Jones potential and elastic deformation of solid surfaces. Greenwood has shown that the load-displacement curve becomes S-shaped at Tabor values of more than one.

A great challenge in modelling the contact of engineering surfaces with adhesion is the irregular nature of the surface topography, which makes the application of analytical models almost impossible. The pioneering work of Fuller & Tabor [9] shed light on the effect of roughness on adhesion by the development of an asperity-based adhesion model. Other significant contributions in the field were reported by Persson & Tosatti [10] who used the self-affine fractal properties of the surfaces and showed the dependency of adhesion on the fractal dimensions.

All the above-mentioned theoretical works have led to significantly increased understanding of the nature of adhesive forces on the contact of surfaces. However, they lack deterministic capabilities to account for the interactions of real surface topographies. In recent years, an increase in computational power has resulted in the development of advanced numerical models that can calculate the adhesive contact of deterministic surface topographies. In a recent contact mechanics challenge, Müser *et al*. [11] presented and compared the results of different numerical approaches for calculation of the adhesive contact of a pre-defined experimentally measured surface roughness. They have shown that numerical approaches such as the boundary element method (BEM) [12], all-atom molecular dynamics (MD) [13] and boundary value methods (BVM) [14] can successfully calculate the contact problem with adhesion. In recent years, there have been numerous works considering the contact of rough surfaces with adhesion. Rey *et al*. [15] developed a BEM-based contact mechanics model based on fast Fourier transforms (FFT) by minimizing the potential energy that is the sum of elastic energy and adhesive energy. Solhjoo & Vakis [13] have developed an MD model using the embedded atom method (EAM) that simulates surface roughness with atoms and gives a high accuracy in contact area calculations and surface pressure, although time-consuming and limited with the number of atoms considered for simulations. Pastewka & Robbins [16] developed a Green's function MD simulation to calculate

the non-adhesive contact of rough surfaces and proposed a criterion for macroscopic adhesion based on the geometry and material.

Other significant contributions were made by Ciavarella *et al.* in a series of articles [2,17,18]. They correlated the bearing area model (BAM) and geometrical intersections to adhesion via a simple mathematical description [19]. The model was reported to be valid for an intermediate range of Tabor parameters. Pohrt *et al.* [20–22] developed a BEM contact mechanics model that used a mesh-dependant detachment criteria for adhesive contact of rough surfaces that was based on the solution of non-adhesive contacts. Ghanbarzadeh *et al*. [23] used the same model and predicted the bouncing behaviour of elasto-plastic and adhesive solids and showed the significance of the effect of roughness in increasing energy dissipation. Bazrafshan *et al*. [24] developed a BEM-based contact mechanics model and incorporated adhesive interactions by means of Dugdale approximation and later studied the effect of roughness and adhesion on the stick/slip of dissimilar materials [25]. Medina & Dini [12] developed a deterministic adhesive contact model using multi-level-multi-integration (MLMI) and implemented adhesion by directly using Lennard-Jones potentials and integrating that over the length of computational nodes to better represent adhesive pressures and to avoid convergence issues due to the nonlinear behaviour of the Lennard-Jones potential.

As discussed, the literature contains extensive and continuously evolving research in the mechanics of contacts in the presence of surface roughness and adhesion. Computational models are becoming increasingly more efficient such that it is now possible using a desktop PC to solve a contact problem in a reasonable time. This paper represents an advancement in the fully deterministic calculation of normal contact of rough surfaces with adhesion by directly using Lennard-Jones potential fields and integration methods over a surface area around the computational nodes to offer an efficient and highly accurate computational model for contact mechanics with adhesion. The model is an advancement to the line integral model developed by Medina & Dini [12] that considered the integration in one dimension. The main aim of the paper is to present this new mathematical model and to show the capabilities of the model by comparing the results with already existing literature. The validity of the model is tested for the case of smooth surfaces and results are compared with the results of Greenwood [8]. The strength of the model to capture the rough surface adhesive contact is also tested by reproducing the results of the contact mechanics challenge reported by Müser *et al*. [11]. Also the idea that the RMS slope of surface roughness is important in determining the adhesion force has been highlighted by the model and a recent theory proposed by Li *et al*. [22] based on a modified Johnson parameter has been tested. Furthermore, a comparison with the model of Ciavarella [26] is made. The method presented here can also be applied to cases where surface geometries are given by analytic functions such as the case of parabolic or spherical geometries by only integrating the height functions with respect to X and Y lateral dimensions. The theory of the model is presented in §2 followed by results and discussion in §3.

2. Theory

(a) Non-adhesive normal contact

The model uses a contact mechanics solver developed previously for non-adhesive contact of rough surfaces using a BEM approach and incorporating FFT for numerical efficiency. When two engineering surfaces with roughness come into contact, due to the inhomogenous nature of the surface roughness, a small proportion of the nominal contact area will sustain the load, known as the real area of contact.

The composite deformation of the surfaces $u_e(X, Y)$ due to the applied load of $p(X, Y)$ can be calculated by the linear convolution according to Boussinesq–Cerruti theory:

$$u_e = K * p_d = \int_{-\infty}^{+\infty} \int_{-\infty}^{+\infty} K(X-\xi, Y-\eta) p(\xi, \eta)\, \mathrm{d}\xi\, \mathrm{d}\eta, \tag{2.1}$$

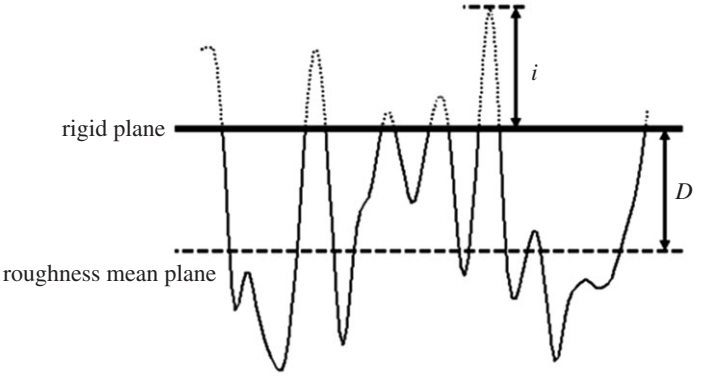

Figure 1. Schematic of the contact of rough surfaces.

in which x and y are two-dimensional coordinates, K is the convolution kernel and can be calculated from the half-space approximation as the following:

$$K(X-\xi, Y-\eta) = \frac{1}{\pi E^*} \frac{1}{\sqrt{(X-\xi)^2 + (Y-\eta)^2}}, \tag{2.2}$$

where E^* is the composite elastic modulus of both materials $(1/E^* = (1-{\nu_1}^2)/E_1 + (1-{\nu_2}^2)/E_2)$. Here, ν_1, ν_2, E_1 and E_2 are the Poisson's ratio and Elastic Moduli of materials 1 and 2, respectively. For the contact of two rough surfaces, one can consider the composite roughness of the two contacting surfaces and a rigid plane to calculate the contacting points [27]. By movement of the rigid body in the normal direction, the interference (i) between the contacting surfaces can be obtained (figure 1). For the nodes experiencing contact, the elastic deformation must be equal to the body interference and the pressure is generated at the asperity. The summation of the pressures on the nodes must also be equal to the applied load. Therefore, the set of equations for the contact of rough surfaces is as follows:

$$u_e(X,Y) = i(X,Y) = H(X,Y) - D(X,Y) \quad \forall (X,Y) \in A_e, \tag{2.3a}$$

$$p(X,Y) > 0 \quad \forall (X,Y) \in A_e \tag{2.3b}$$

and

$$W = \iint p(X,Y)\,\mathrm{d}X\,\mathrm{d}Y, \tag{2.3c}$$

where i is the asperity interference, H is the composite surface roughness height, D is the distance between the reference plane and the rigid plane and W is the total applied load. The separation of asperities can be defined by $g(X,Y) = D(X,Y) - H(X,Y) + u(X,Y)$.

(b) Adhesion model

In this paper, adhesive pressures are calculated at the areas of asperity separation by means of direct implementation of the Lennard-Jones potential. The potential was first defined by John Lennard-Jones in the following format:

$$v = 4\epsilon \left[\left(\frac{\sigma}{r}\right)^{12} - \left(\frac{\sigma}{r}\right)^{6} \right], \tag{2.4}$$

where v is the inter-atomic potential, ε is the depth of the potential wall, σ is the distance between particles at which the potential becomes zero and r is the finite separation of the two particles. Differentiation of equation (2.4) with respect to r (separation) results in the determination of the

force applied on the particles. Similarly, if potential energy per unit area is differentiated with respect to r, an expression for pressure is determined as in the following:

$$p(z) = \frac{8w_0}{3z_0}\left\{\left(\frac{z_0}{z}\right)^9 - \left(\frac{z_0}{z}\right)^3\right\}, \tag{2.5}$$

where w_0 is the work of adhesion and can be measured experimentally or is calculated by integration of pressure with respect to separation from $z = z_0$ to $z = \infty$:

$$w_0 = \int_{z_0}^{\infty} p(z)\,\mathrm{d}z, \tag{2.6}$$

where z_0 is the equilibrium separation when the potential is at its maximum and the adhesive force (pressure) is zero and z is the separation distance between two planes.

Equation (2.5) is valid for the case of two parallel planes with a separation distance z. In order to be able to use the above formulation in a discretized boundary element formulation, there is a need to approximate the adhesive pressure over the area around a computational node. This is not a straightforward task and a proposed way to approach this is presented in the following paragraph.

To facilitate the approximation of the adhesive pressures, it is necessary to consider the configuration of the computational nodes in BEM. Figure 1 represents the cross section of the roughness profile only in one dimension. The real surface topography is a two-dimensional matrix with every element representing the surface height of a computational node. Figure 2 shows a discretized surface with point 1 being the point where surface tensions are being calculated with respect to equation (2.5). Substituting the separation value (z) of the node 1 in equation (2.5) results in a value of pressure (two black squares in figure 2), which is not representative of the pressure in the computational domain for point 1 (dashed square around point 1). The dashed square in figure 2 represents the BEM domain for one computational node at which the pressure is assumed to be constant. Points A, B, C and D (shown by blue dots) are the points of interest at which the separation will largely affect the tensile pressure at point 1. A significant amount of information is missed (if only the pressure at point 1 is taken into account) at the edges of the computational node (points A, B, C and D) due to the shape of the Lennard-Jones potential. Figure 2 shows how separation values at points A, B, C and D affect the integral value of tensile stress over the line integrals moving in X and Y directions.

This problem is valid for movements in both X and Y directions on the surface. In order to overcome this issue, an approximation is needed to integrate the profile of the Lennard-Jones potential in both X and Y directions and calculate the two-dimensional average of the pressure. The Lennard-Jones pressure formulation of equation (2.5) is dependant only on the separation of surfaces in the normal direction and the integration should be carried out in X and Y directions as a surface integral. Therefore, the following formulation is proposed:

$$p(i) = \frac{1}{a^2}\iint p(z)\,\mathrm{d}s, \tag{2.7}$$

where a is the length of the computational elements in X and Y directions, and ds is the differential of the surface representing the surface heights. For the BEM calculations, the surface integral needs to be carried out with respect to X and Y with the following integration:

$$p(i) = \frac{1}{a^2}\iint\left\{f(X,Y,z(X,Y))\sqrt{\left(\frac{\partial z}{\partial X}\right)^2 + \left(\frac{\partial z}{\partial Y}\right)^2 + 1}\right\}\mathrm{d}A, \tag{2.8}$$

where f is a function that we need to integrate on the surface (in this case, the adhesive pressure function), $z(X, Y)$ is the separation function with respect to X and Y coordinates and dA is the differential of the projection area on the XY plane as shown in figure 3. Equation (2.8) considers the changes in the mean value of the adhesive pressure function by the increment of surface area due to roughness. It should be noted that the shape of the surface nodes (in terms of their sharpness, etc.) affect the intensity of the average separation and therefore the average adhesive

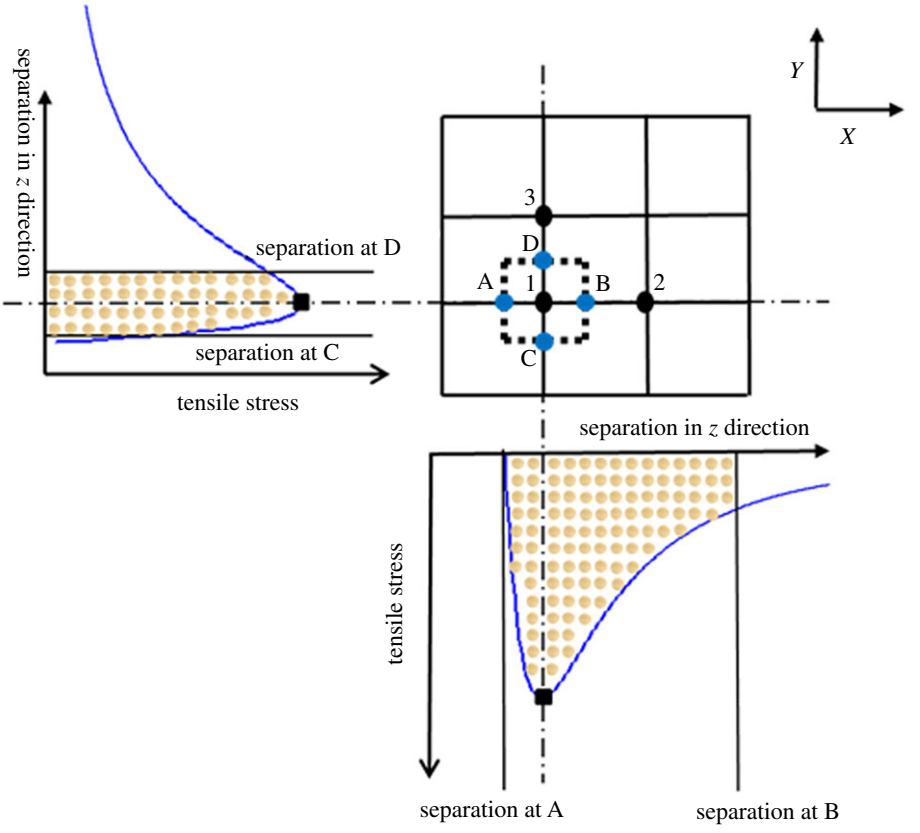

Figure 2. Discretization of the surface in BEM. Point 1 represents the computational node that adhesion pressure is going to be calculated at. (Online version in colour.)

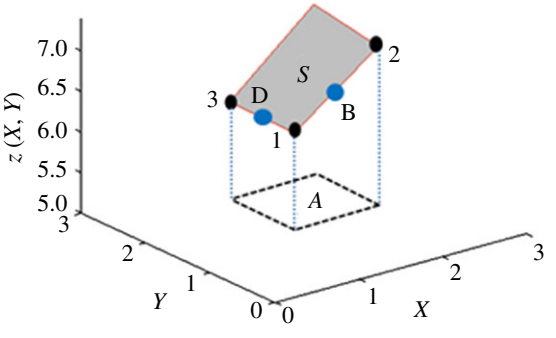

Figure 3. Representation of surface separation and its projection on the XY plane. Points shown are the same as the ones in figure 2. (Online version in colour.)

pressure. We are only able to integrate the separations from point 1 to point 2 in the X direction and from point 1 to point 3 in the Y direction. Ideally, we should integrate from point A to point B in the X and from point C to point D in the Y direction. This is impossible since we do not have information regarding the heights for points A, B, C and D.

Ideally, having a surface integral on the area A would enable calculation of the pressure. That needs the equation of z as a function of X and Y to be determined. This is possible using the

bilinear interpolation technique. However, this will give a nonlinear function of z based on X and Y and the integrating equation (2.8) will be impossible analytically. Instead, by substituting equation (2.5) into equation (2.8) and writing $dA = dXdY$, and knowing that $dX = (dX/dz)\,dz$ and $dY = (dY/dz)\,dz$, the integration can take the form:

$$p(i) = \frac{1}{a^2}\int_{Y_1}^{Y_3}\int_{X_1}^{X_2}\left\{\frac{8w_0}{3z_0}\left\{\left(\frac{z_0}{z}\right)^9 - \left(\frac{z_0}{z}\right)^3\right\}\sqrt{\left(\frac{\partial z}{\partial X}\right)^2 + \left(\frac{\partial z}{\partial Y}\right)^2 + 1}\right\}\left(\frac{dX}{dz}dz\right)\left(\frac{dY}{dz}dz\right), \tag{2.9}$$

in which X and Y stand for the position of points in the X and Y direction and the subscripts represent the nodes of interest. Solving the integral of equation (2.9) results in the adhesive pressure formula for each node to be calculated by

$$p(i) = \left(\frac{1}{a^2}\left(\sqrt{\left(\frac{z_2 - z_1}{X_2 - X_1}\right)^2 + \left(\frac{z_3 - z_1}{Y_3 - Y_1}\right)^2 + 1}\right)\left(\frac{X_2 - X_1}{z_2 - z_1}\right)\left(\frac{Y_3 - Y_1}{z_3 - z_1}\right)\right) \times \int_{z_1}^{z_3}\int_{z_1}^{z_2}\left\{\frac{8w_0}{3z_0}\left\{\left(\frac{z_0}{z}\right)^9 - \left(\frac{z_0}{z}\right)^3\right\}\right\}dz\,dz. \tag{2.10}$$

Knowing that $X_2 - X_1 = Y_2 - Y_1 = a$ and solving the double integration, the final equation is solved as

$$p(i) = \left(\left(\sqrt{\left(\frac{z_2 - z_1}{X_2 - X_1}\right)^2 + \left(\frac{z_3 - z_1}{Y_3 - Y_1}\right)^2 + 1}\right)\left(\frac{1}{z_2 - z_1}\right)\frac{w_0}{3z_0}\right)\left(\frac{4z_0^3}{z_2^2} - \frac{z_0^9}{z_2^8} + \frac{z_0^9}{z_1^8} - \frac{4z_0^3}{z_1^2}\right). \tag{2.11}$$

In order to solve the adhesive problem using equation (2.11), information from the adjacent nodes in X and Y directions (2 and 3) is needed. Therefore the BEM algorithm should start calculating the adhesive pressures from one row (in either X or Y direction) and complete the pressure profile by moving across the columns one by one. It should be noted that equation (2.9) can be used when H or z is represented as a function of X and Y (e.g. for the case of parabolic or spherical smooth contacts an analytical model of adhesive pressures can be developed). This will be the subject of future investigations and is not within the scope of the present paper.

(c) Numerical approach

The non-adhesive contact model explained in §2a should now be modified to account for the adhesive pressures calculated at separated computational nodes using equation (2.11). This needs a careful definition of surface separations between all computational nodes since separation g defined after equation (2.3) has now to accommodate atomic separation z in equation (2.11). Due to the shape of Lennard-Jones potentials, separation less than z_0 will result in high compressive pressures. Since compressive pressures are already calculated using the non-adhesive algorithm of §2a, positive pressures should be truncated out of adhesive calculations. In order to overcome this, a relationship between atomic separation (z) and continuum separation (g) is used as the following [12]:

$$g + z_0 = z. \tag{2.12}$$

This new separation (z) will be used in equation (2.11) to calculate the adhesive pressures. Although this will shift the profile of Lennard-Jones for z_0 to the left, Medina & Dini [12] showed this can be tolerated due to the sharp slope of the shape of the pressure profile. The non-adhesive formulation of equation (2.3) is now converted to an adhesive problem as the following:

$$\begin{aligned} &p_i > 0 && g_i = 0\\ &p_i < 0 \text{ based on equation (2.11)} && g_i > 0.\\ &W = \iint p(X, Y)\,dX\,dY \end{aligned}$$

This new set of equations needs to be solved in an iterative process. Previously, for a non-adhesive contact, pressures less than zero could be simply truncated out of simulation by

replacing them with zero pressures. For adhesive contact, the negative pressures will be present and they disturb the gap and elastic deformation balance. Solving the new contact problem with adhesion needs a robust numerical algorithm since the introduction of negative (adhesive) pressures can easily lead to difficulty in convergence. A new numerical algorithm is presented here that was shown to work for all contact cases including low and large Tabor parameters for both smooth and rough surfaces. The detailed description of the algorithm is given below:

— An initial contact pressure distribution is assumed on the entire surface that is a combination of the positive (p_c- compressive) and the negative (p_a- adhesive) pressures. $p_{\text{total}} = p_c + p_a$. Selection of a suitable initial adhesive pressure is critical in our algorithm and defines how quickly the final solution is converged. It was shown that a constant negative pressure of $p_a = -(16w_0/9\sqrt{3}z_0)$ will result in the quickest and most efficient computation for unloading of contact. For loading (jumping into contact), we start from zero adhesion.
— Calculate the positive pressures using equation (2.3) and replacing negative pressures by zero. The total pressure p_{total} is used to calculate the surface deformations in this stage. The relaxation in this stage updates the positive pressures with the following process: $p_c = p_c - k_{c-\text{relax}} \times g$ where $k_{c-\text{relax}}$ is the relaxation factor for positive pressures and g is the separation at each node. Values in the range of 0.00000001 and 0.01 were used depending on the elastic properties of surfaces. This relaxation factor was optimized independently only for positive pressures.
— The separation at points of zero pressure was calculated and adhesive pressures ($p_{a-\text{new}}$) were calculated at every node using equation (2.11).
— The residuals of surface points were calculated in a new iteration loop where only adhesive pressures p_a were relaxed using a new relaxation coefficient as the following: $p_a = p_a + (k_{a-\text{relax}} \times g) \times (p_{a-\text{new}} - p_a)$ where $k_{a-\text{relax}}$ is the relaxation factor for adhesive pressures and is independent of $k_{a-\text{relax}}$. This coefficient is in the range of 0.0000001 and 0.1 and dependant on the local Tabor parameter. Here, we used the inverse root mean square curvature, which can be interpreted as the local radius of curvature to identify the local Tabor parameter in the presence of roughness. The residuals and surface deformations were calculated by the total pressure p_{total} being updated as $p_{\text{total}} = p_c + p_a$ and new surface deformations were calculated.
— This process was undertaken until a convergence was achieved between p_a and $p_{a-\text{new}}$. It should be noted that the relaxation of positive and negative pressure was carried out independently in two interconnected loops. The loop for the positive pressure calculations was done prior to the calculation of negative pressures and was carried out in every adhesive pressure loop.

The convergence criteria in this model were set as the average of the residuals for positive pressures to be less than $z_0 \times 10^{-6}$.

A schematic of the algorithm is represented in figure 4.

3. Results

(a) Simulation of smooth surfaces

For the sake of model validation, the case of smooth spheres with a range of Tabor parameters has been studied and the results of dimensionless load ($W/2\pi R^* w_0$) versus dimensionless approach (α/z_0) were compared with the existing theories. It is tricky to capture the adhesive contact behaviour of surfaces for Tabor parameters ranging from $0.1 < \mu < 3$ since they are describing the transition from DMT to JKR theories. In this case, a comparison with the model of Greenwood [8] is represented. The Tabor parameter is defined as $\mu = R^{*1/3} w_0^{2/3} / E^{*2/3} z_0$ where R^* is the equivalent radius of curvature and for the case of a sphere on a flat surface is the radius of

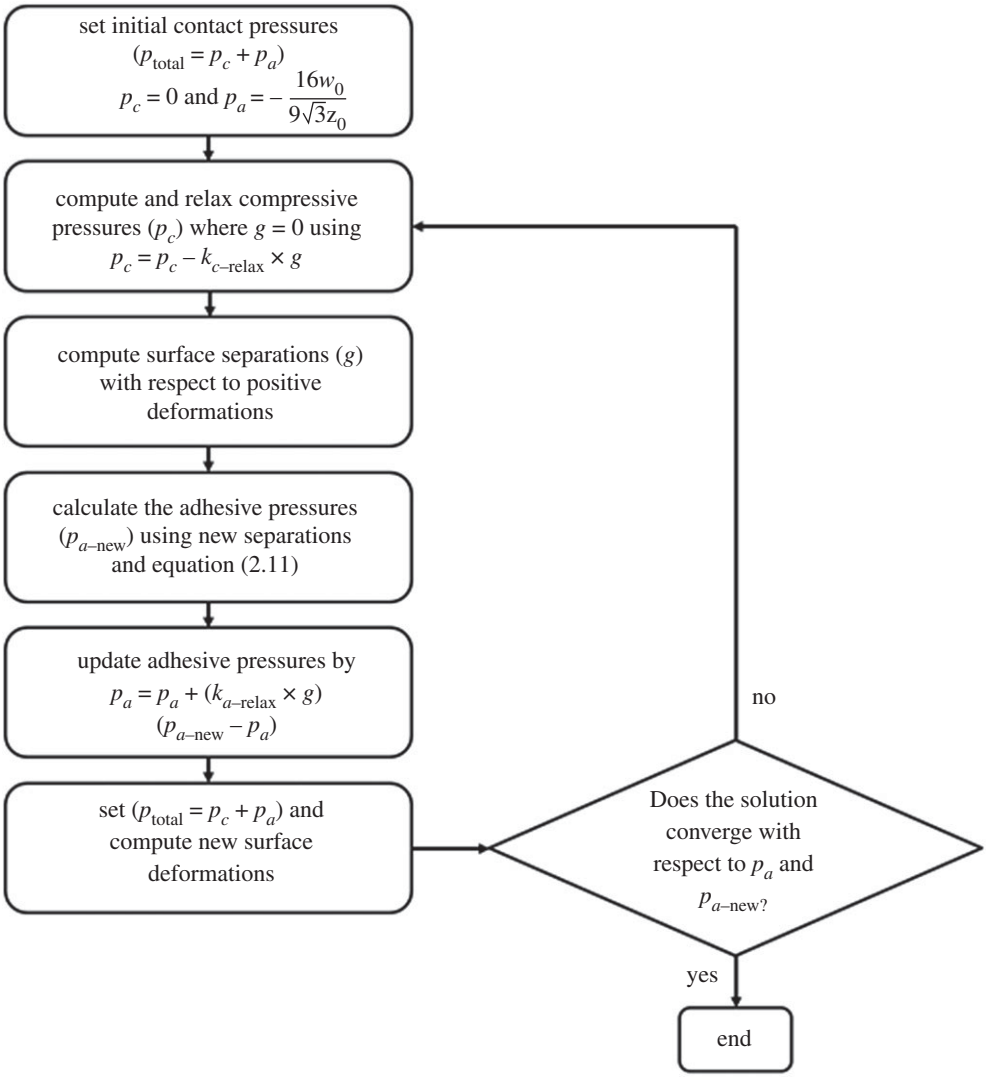

Figure 4. Schematic of the numerical algorithm.

the curvature of the sphere. Figure 5 shows the comparison of our model with the model of Greenwood at values of $\mu = 0.1, 0.2$ and 0.3, and figure 6 shows the comparison for $\mu = 1, 2$ and 3 where a good agreement is observed. The simulations can capture the adhesive pressures for negative values of separation. For the case of higher Tabor parameters (figure 6), Greenwood has shown an S-shape behaviour in the loading-unloading curve. These phenomena can be captured by the current numerical model if two different simulations (loading and unloading) are conducted. However, the simulation cannot capture some part of the adhesive pressure between loading and unloading. This is due to the nature of these numerical models that need a certain value of separation as input to the model (displacement controlled) and the model cannot give two values of pressure for the same separation (inevitable in S-shape profile). This would become possible by a force-controlled numerical approach. Greenwood has used a solution by fixing the displacement at the centre of the contact. The arrows on the load-separation curve in figure 6 show if the data have been obtained in loading or unloading cycles. It should be noted that convergence time increased as the Tabor parameter increased and it is due to higher adhesive pressures and higher disturbance of the deformations of positive pressures (non-adhesive case). An example of

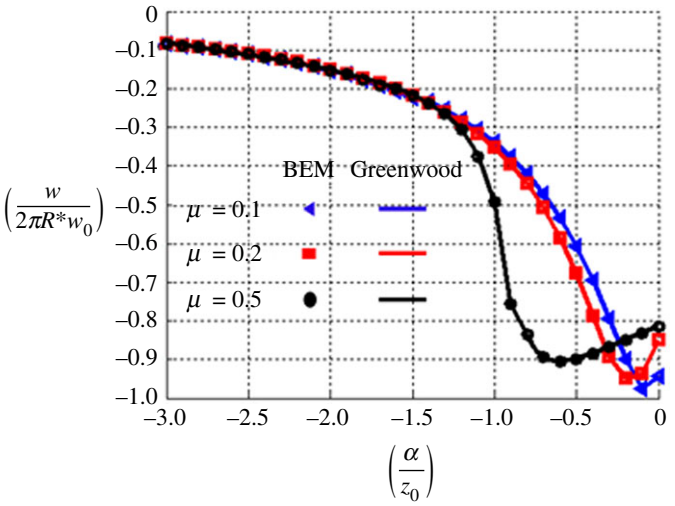

Figure 5. Comparison between the current model and Greenwood's model for small values of Tabor parameters. Dimensionless load is plotted against dimensionless approach. (Online version in colour.)

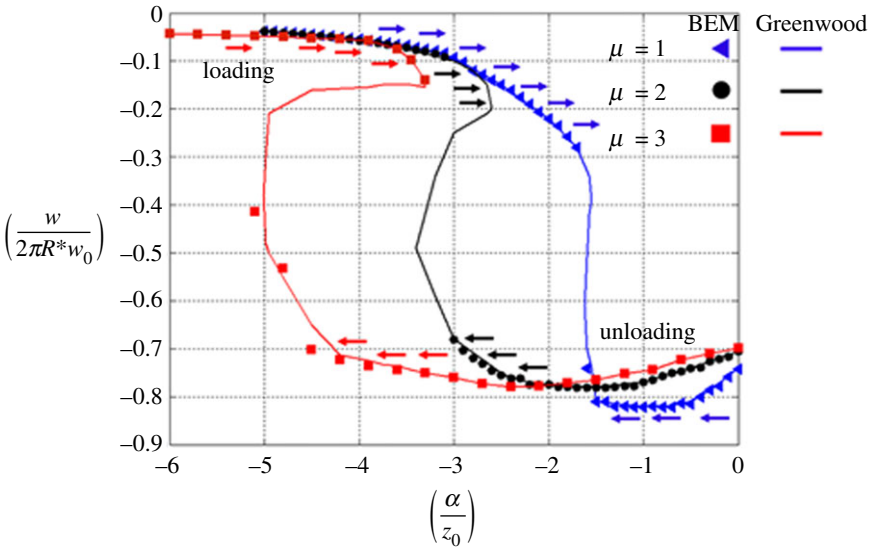

Figure 6. Comparison between the BEM model and the Greenwood model for Tabor parameters of $\mu = 1$, 2 and 3. Dimensionless load is plotted against dimensionless approach. (Online version in colour.)

the contour of contact pressure as well as cross section of the total pressure in the middle plain is reported in figure 7.

(b) The contact mechanics challenge

In December 2015, Martin Müser introduced a contact mechanics challenge where a pre-defined self-affined surface was created, and scientists were asked to use their own in-house numerical techniques to calculate the contact between the surface and a rigid flat surface. The results presented in a published paper [11] show a reasonable agreement between numerical results (e.g.

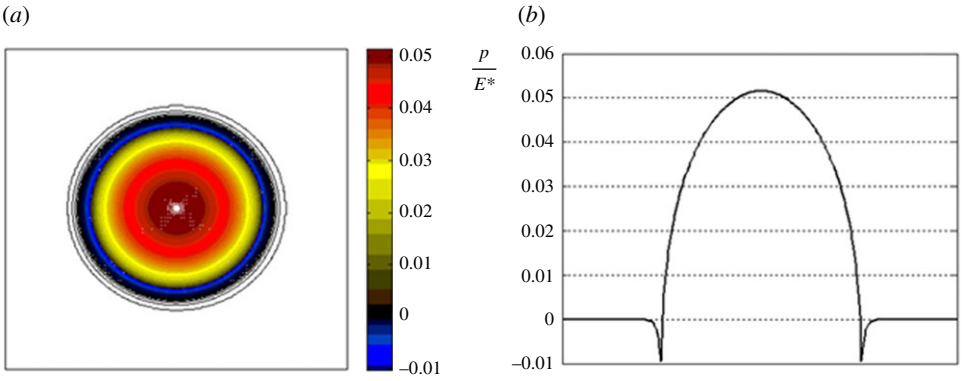

Figure 7. Representation of (*a*) the contour of contact pressure and (*b*) cross section of the pressure profile for the case of a smooth plane in contact with a rigid indenter. (Online version in colour.)

Green function molecular dynamics [GFMD], all-atom MD, FFT-BVM, etc). The purpose of this section is to use the same surface used in [11] and to reproduce the results with the numerical model presented in this paper for comparison. Initially, the parameters used in the challenge will be summarized here. The surface was normalized to have a root mean square gradient of $\bar{g} = 1$, minimum height of zero and a maximum of 5.642 µm, and the surface was representing an area of 0.1 mm × 0.1 mm. The inverse root mean square of the curvature which can be used as a typical local radius of curvature was defined as $R^* = 60$ nm. In addition, the equivalent elastic modulus was set as $E^* = 25$ MPa, the work of adhesion was set as $w_0 = 50\,\mathrm{mJ\,m^{-2}}$ and the equilibrium separation was $z_0 = 2.071$ nm. The simulations were carried out using the current BEM model and adopting the parameters in the challenge. The results for the relative contact area against normalized pressure and the gap distribution in the middle plane of the contact have been reproduced. Figure 8 shows the comparison of the current model (BEM) with two selected numerical results (i.e. GFMD and FFT-BVM from the challenge). The result shows good quantitative agreement between BEM and the result of the challenge. The x-axis represents the average of contact pressure across the whole nominal area normalized by the $E^*\bar{g}$, and the y-axis is the ratio of contacting areas with the total nominal area. Figure 9 presents the profile of the gap in a cross section in the middle of contact ($x = 50$ µm) and compares the results of the current model with GFMD simulations presented in [11] and a good agreement is found. The small discrepancy in the results could be due to the differences in the resolution of the simulations. The simulations carried out in this model use a discretization of 4096 × 4096.

(c) Effect of roughness

Numerical methods such as the one developed in this paper are ideal for studying the contact behaviour of deterministic rough surfaces. Here, we have generated rough surfaces with self-affine properties to examine the effect of different surface characteristics on the real area of contact and stickiness of surfaces. The pull-off force (the force needed to completely separate the surfaces) and the contact area ratio were also plotted for different surfaces at different Tabor parameters. Surfaces are generated using the power spectrum density as reported by Persson [28]. Random numbers were used along with Fourier transforms of the height function ($\tilde{h}(q)$). The height spectrum $C(q)$ was defined as

$$C(q) = C(q_r) \times \begin{cases} 1 & \lambda_r < \dfrac{2\pi}{q} \le L \\ \left(\dfrac{q}{q_r}\right)^{-2(1+H)} & \lambda_s \le \dfrac{2\pi}{q} < \lambda_r \\ 0 & \end{cases}. \tag{3.1}$$

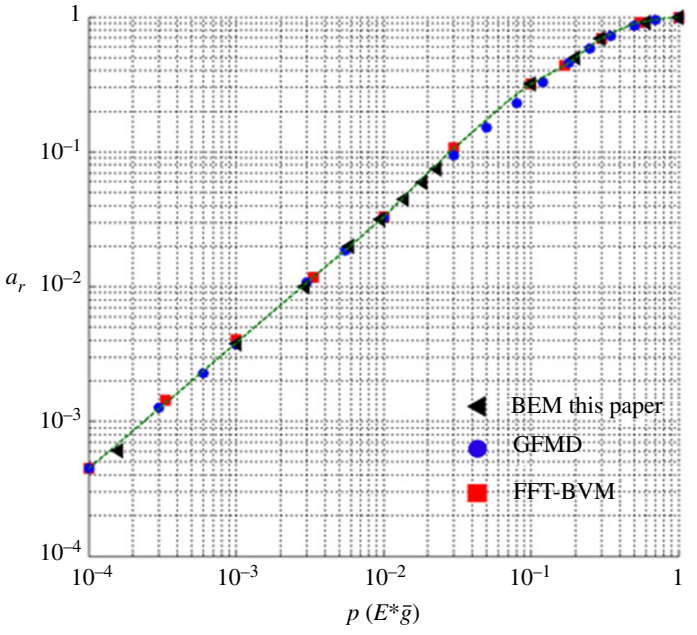

Figure 8. The relative contact area (a_r) against normalized average pressure ($p/E^*\bar{g}$) and the comparison with the contact mechanics challenge [11]. GFMD and FFT-BVM have been chosen for comparison. (Online version in colour.)

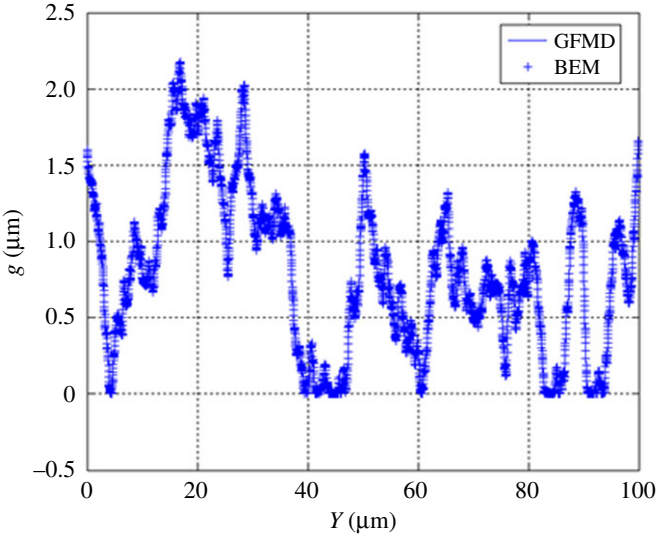

Figure 9. Gap distribution of deformed surfaces (g) at a cross section in the middle of contact ($X = 50$ μm in the contact mechanics challenge problem definition). The results of BEM in this work are compared with the GFMD results from [11]. (Online version in colour.)

In which λ_r is the roll-off wavelength, λ_s is the short wavelength cut-off, L is the length of the surface in each dimension, $q_r = 2\pi/\lambda_r$ and H is the Hurst parameter, which is calculated by $H = 3 - D_f$ where D_f is the fractal dimension. All the surfaces generated with this method have a mean of zero.

Müser [29] has shown that the formula for relative contact area first introduced by Pastewka & Robbins [30] can accurately capture the non-adhesive contact behaviour of rough surfaces and introduced a new formula by improving the Pastewka and Robbins criteria using a new equation for contact area by eliminating the mean-field approximation.

$$a_r(k\tilde{p}) = \pi a_0^2 \left(1 - \frac{1}{2k^2\tilde{p}^2}\right) \mathrm{erf}(k\tilde{p}) + \frac{\exp(-k^2\tilde{p}^2)}{\sqrt{\pi}k\tilde{p}}. \tag{3.2}$$

In equation (3.2), a_r is the relative real contact area, k is a number that is often two for real engineering surfaces, $\tilde{p}$ is calculated by $\tilde{p} = 3L/4\sqrt{\pi}E^*\bar{g}a_0^2$ and is a physical representation of the average contact pressures, L is the total applied load on the nominal area, $\bar{g}$ is the root mean square gradient of surface roughness and a_0 is the radius of the nominal contact area. Equation (3.2) is used in this work to analytically predict the contact area in the case of adhesion-less contact and the BEM is used to predict the contact area for adhesive contact. The aim of this section is then to see the effect of adhesion on the real contact area for rough surfaces. Figure 10 shows the comparison between the adhesive model ($\mu = 3$) presented in this paper and the non-adhesive theory of Müser [29]. The discrepancy of adhesive and non-adhesive contacts is more significant for higher values of the Tabor parameter. Results clearly show that adhesion is playing an important role in increasing the relative contact area as expected. The other point to highlight is that the model—with a very good quantitative agreement—can follow the trend of area of contact in the presence and absence of adhesion. This interesting numerical finding is valid for both values of root mean square gradient of surface roughness. This means that for cases with a larger radius and softer materials the real contact area is significantly affected by adhesion. Physical problems such as contact and friction of rubbers, contact of biomaterials, cartilages and cells and contact of viscoelastic solids can be largely dependent on adhesion. Ignoring surface roughness and adhesion in such areas will considerably misrepresent the contact mechanics and evaluation of the corresponding friction and wear. For instance, for small values of average pressure ($\tilde{p}$), real area for the case of adhesive contact is larger than the area of non-adhesive contact by a factor of 2 or 3. This is a large underestimation of the contact area, which can eventually underpredict friction and wear by the same factor. This highlights the importance of models such as the one developed in this work to deterministically calculate real contact area and pressure distribution in the presence of adhesion.

(d) Effect of roughness on the pull-off force

In the adhesive contact of surfaces, when the approach of the bodies is negative, adhesive forces will deform the surfaces, and there may be body interference between solid surfaces, which in turn causes compressive pressures. The area, in which the compressive pressures still exists is the contact area. The minimum negative force in the process of separating the surfaces is called the pull-off force. This is the minimum negative force required to completely separate the surfaces. In this section, the effect of surface roughness and the Tabor parameter on the pull-off force calculated by BEM is presented. The results are then compared with the numerical results produced by Medina & Dini [12] to see how results from a more complete surface integral method will differ from a line integral approach. The simulation parameters are set as ($R^* = 100\,\mu\mathrm{m}$, $E^* = 50\,\mathrm{GPa}$, $z_0 = 0.3\,\mathrm{nm}$, $w_0 = 0.29\,\mathrm{J/m^{-2}}$ and $w_0 = 0.075\,\mathrm{J/m^{-2}}$) in order to get Tabor parameters 5 and 2, respectively, and the results are plotted in figure 11.

It should be noted that the main part of the results section of this paper looks at validation of the new mathematical model and the algorithm proposed, with the existing theories in the literature for both smooth and rough surfaces. This is to show how effectively Lennard-Jones potentials could be applied on a rough surface in BEM to predict adhesion in contact mechanics. In order to further study the effect of roughness parameters on adhesion, we have extended our study to investigate the effect of RMS slope $\bar{g}$ on the adhesion. Simulations are carried out with the same root mean square roughness (R_q) of $2z_0$ but different $\bar{g}$ values and the effect of $\bar{g}$ on the pull-off force were investigated.

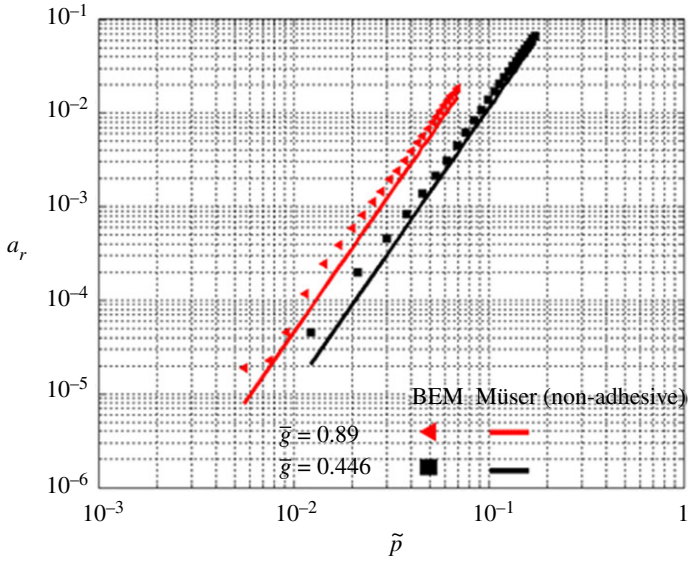

Figure 10. Comparison between the theory of Müser [29] for non-adhesive contact of rough surfaces and the BEM for adhesive contacts. Relative contact area is plotted against pressure ($\tilde{p}$) for two values of $\bar{g}$. (Online version in colour.)

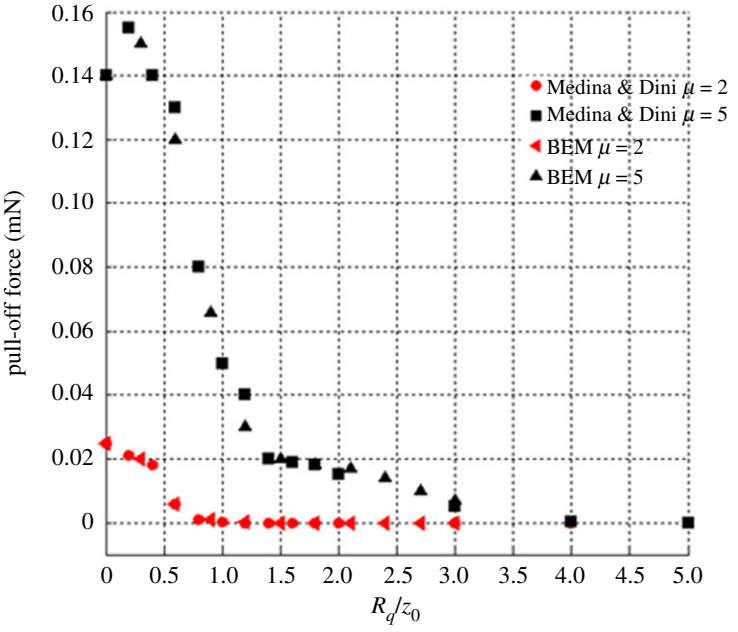

Figure 11. Effect of R_q on the pull-off force for randomly rough surfaces and the comparison with the results of Medina & Dini [12]. (Online version in colour.)

Figure 12 represents the results when the root mean square roughness of the surface is constant and only the mean square gradient of roughness ($\bar{g}$) is altered to see the effect on the force needed to separate surfaces. The results clearly show that increasing the $\bar{g}$ will result in decreasing the pull-off force and this is independent of the R_q value of the surface roughness. The value of $\bar{g}$

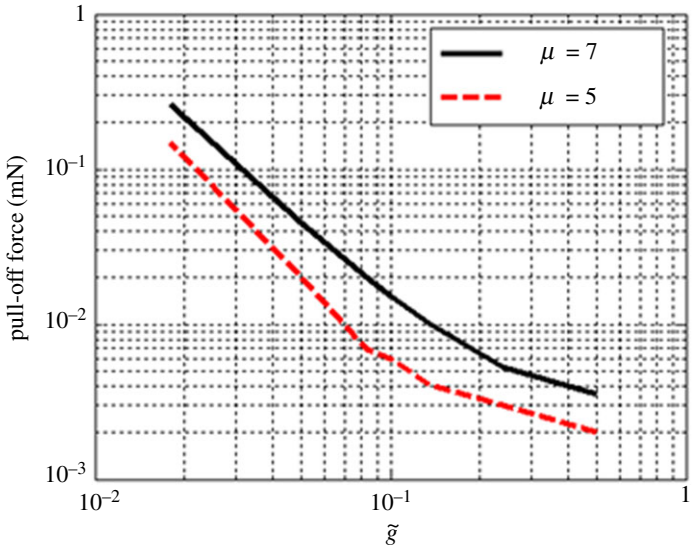

Figure 12. Effect of root mean square gradient of surface roughness on the magnitude of pull-off force for the case of $\mu = 5$ and $\mu = 7$, $R_q = 2z_0$. (Online version in colour.)

represents how sharp or blunt the surface asperities (at least at the resolution that topography is defined) are, which in turn affects the separation of surfaces near the edge of contact.

The simulations presented in this paper study the effect of surface topography on the adhesive pressures in the contact of nominally flat surfaces. The effect of adhesion is shown to be important in determination of real contact area. Results of figure 10 show the difference of the relative contact area in the case of adhesive contact with the case of non-adhesive contact reported by Müser. It also proves the fact that adhesion increases the real area of contact as expected. It was shown previously that increasing the root mean square of surface roughness will reduce the effect of adhesive pressures on the surfaces in contact. This is due to higher separation of surface points. In addition, rougher surfaces will experience higher compressive pressures at the point of higher topography peaks and the small adhesive pressures will be negligible compared with the compressive ones. The pull-off force needed to separate surfaces generally decreases as the root mean square roughness increases.

It should be highlighted that we have investigated the effect of these parameters (R_q and $\bar{g}$) and have numerically shown the importance of both. The recent theoretical works of Ciavarella *et al.* [2,26,31] have highlighted alternative surface and material parameters responsible for the area of contact and discussion around stickiness criteria was made. They used different independent theories (BAM, Persson & Tosatti [10]) along with DMT theories previously reported by Persson & Scaraggi [32]. They have shown that macroscopic features of surface roughness such as R_q and the low wavevector cut-off of surface roughness and the ratio of work of adhesion and the equivalent Young's modulus are important parameters for stickiness. This is interesting and we believe our results do not contradict with the criteria of Ciavarella. We have therefore carried out an investigation to include the effect of both RMS and RMS slope on the adhesive force calculations of rough surfaces. Recently, Li *et al.* [22] have demonstrated the effect of the Johnson parameter [33] in the adhesive contact of wavy surfaces. They have introduced a modified version of the Johnson parameter that considers the fractal properties of rough surfaces and argued that the adhesion between rough surfaces is dependent on this new parameter for larger values of Tabor parameter (JKR-limit). The modified version of the Johnson parameter (α^*) was formulated as

$$\alpha^* = \left(\frac{4w_0 q_1^{0.8H-1}}{\pi E^* h^2 q_0^{0.8H}} \right)^2, \tag{3.3}$$

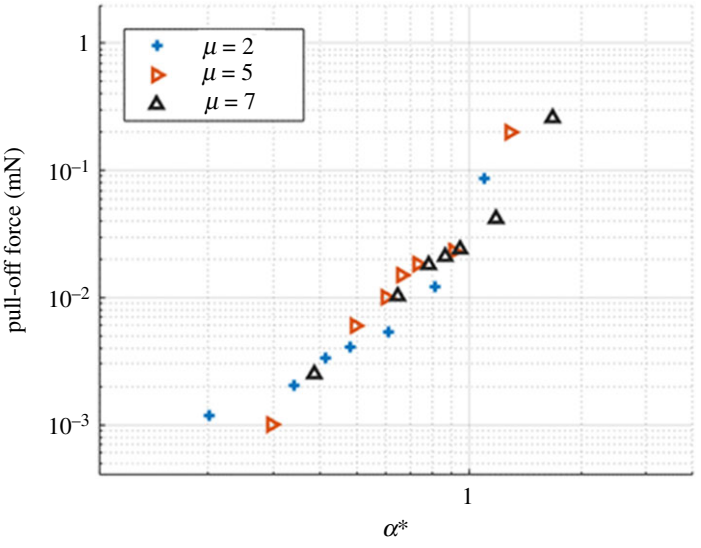

Figure 13. The effect of the modified Johnson parameter on the pull-off force for three values of Tabor parameter ($\mu = 2$, 5 and 7). (Online version in colour.)

in which H is the Hurst exponent of the fractal surface, h is the RMS roughness and q_0 and $q_1$are the smallest and largest wavevectors, respectively. We have plotted the pull-off force with respect to the modified Johnson parameter (α^*) for three values of Tabor parameter ($\mu = 2$, 5 and 7) and the results are presented in figure 13. Results indicate that normalizing our pull-off force calculations with respect to the modified Johnson parameter results in very similar values of the pull-off force. It should be noted that Persson & Scaraggi [32] and Ciavarella [19] have shown that the pull-off force is almost independent of the large wavevector component. Our results show that for this new modified dimensionless parameter that includes both RMS and RMS slope, small and large wavevectors could be a reasonable but not fully comprehensive stickiness criteria for the adhesion of rough surfaces with fractal properties in JKR-limit. This is because our results show small discrepancies at different Tabor parameters (JKR-limit), which suggests that the parameter could somehow be modified. Our simulation data are also in line with the results of Li *et al*. [22], which showed the same dependency.

In order to test the numerical model with other stickiness criteria, we have used the theory of Ciavarella [26], which was based on the BAM model. In his model, Ciavarella introduced new adhesion criteria along with those of Persson & Tosatti [10] and has shown that both models although from completely different origins, predict very similar stickiness criteria. The stickiness criteria of Ciavarella was reported as the following:

$$R_q < \sqrt{\beta \lambda_L I_a}, \tag{3.4}$$

in which β is 0.6 in his theory, λ_L is the large wavelength of the surface roughness and I_a is (w_0/E^*). These criteria suggest that only RMS roughness and the large wavelength of roughness (small wavevector) are responsible for stickiness. In order to compare our results with this theory, we have plotted our pull-off force calculations against $(R_q^2 E^*/\lambda_L w_0)$ for different cases at Tabor parameters of $\mu = 2$, 5 and 7 and the results are plotted in figure 14. It is interesting to see that the new parameter is a good stickiness criteria for this range of Tabor parameter since the results of pull-off force against this stickiness parameter matches almost perfectly for all three values of Tabor parameter. This suggests that equation (3.4) (Ciavarella's stickiness model) is the most accurate and reasonable stickiness criteria based on our simulations.

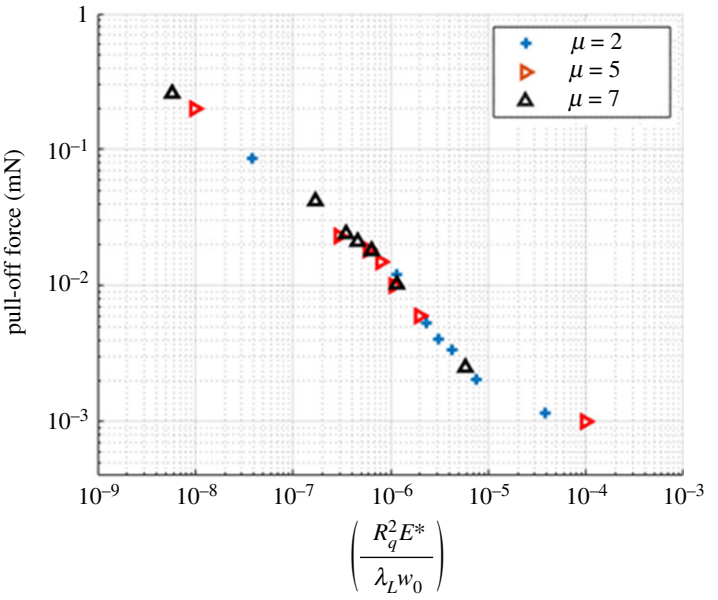

Figure 14. Pull-off force against the stickiness criteria of Ciavarella [26] for $\mu = 2$, 5 and 7. (Online version in colour.)

We believe our model could be a platform for the future development of adhesion models for real rough surfaces and more robust stickiness criteria for a wider range of materials could be achieved.

4. Conclusion

This paper presents the development of a BEM model for contact mechanics of rough surfaces. Adhesion is considered by means of inter-atomic Lennar-Jones potential and a new surface integration approach is incorporated. The model extends the model of Medina and Dini where a line integration of the Lennard-Jones potential was developed. The model shows very good quantitative agreement with the model of Greenwood for medium range Tabor parameters and reproduces exact solutions of the contact mechanics challenge introduced by Müser. The deterministic nature of the model enables us to analyse the adhesive contact of surfaces with any complex geometry and investigate the local pressures and deformations at micron- and nano-scales. Therefore the effect of roughness on the adhesion is studied with a focus on the root mean square gradient of roughness and the following conclusions are drawn:

— A new mathematical equation is developed in this work to evaluate adhesion of rough surfaces and can be used in BEM simulations. The incorporation of the mathematical equation is simple and the algorithm used in this work is very efficient.
— It was numerically shown that inclusion of adhesion in the deterministic contact calculations of rough surfaces affects the real contact area ratio. This was shown by comparing the numerical results of BEM developed in this paper with those of the analytical model developed by Müser. It was revealed that the root mean square gradient of roughness not only affects the real area of contact in the non-adhesive case, but also affects the area of contact in the case of adhesive contact.
— We have presented that not only the R_q value can significantly reduce the adhesion effect, but also the root mean square gradient of surface roughness can significantly affect the adhesive forces. Higher root mean square gradient results in lower adhesive force and

lower pull-off force are needed to separate surfaces. This is believed to be due to the difference in the real area of contact caused by the shape of asperities.

— We have investigated the effect of the modified Johnson parameters (that include both fractal properties and RMS) on the stickiness of rough surfaces and have shown that this dimensionless parameter could be a reasonable but not fully comprehensive stickiness criteria for the contact of rough surfaces.

— Furthermore, we have shown that the criteria introduced by Ciavarella almost perfectly matches our simulation results and by far is the best stickiness criteria based on our simulations.

Ethics. There are no ethical considerations required for this research.

Data accessibility. The data published in this paper including the contact mechanics code are accessible upon request from the corresponding author.

Authors' contributions. A.G. developed the numerical model, ran the simulations, analysed and interpreted the data and drafted the paper, approved the final version and is accountable for the paper. A.N. analysed and interpreted the data, contributed to the discussion and revision of the article and gave final approval. M.F. carried out simulations and contributed towards the final discussion.

Competing interests. We declare we have no competing interests.

Funding. This work is supported by the Engineering and Physical Sciences Research Council (grant no. EP/001766/1) as a part of 'Friction: The Tribology Enigma' Programme Grant (www.friction.org.uk), a collaboration between the Universities of Leeds and Sheffield.

Acknowledgements. The authors are grateful to Dr Mark Wilson from the University of Leeds for kindly sharing his thoughts on the mathematical rigour of the developed model. The authors are also thankful to Professor Martin Müser from Saarland University for kindly sharing the raw data reported in the contact mechanics challenge paper.

References

1. Israelachvili JN. 2015 *Intermolecular and surface forces*. New York, NY: Academic Press.
2. Ciavarella M, Joe J, Papangelo A, Barber J. 2019 The role of adhesion in contact mechanics. *J. R. Soc. Interface* **16**, 20180738. (doi:10.1098/rsif.2018.0738)
3. Johnson KL, Kendall K, Roberts A. 1971 Surface energy and the contact of elastic solids. *Proc. R. Soc. Lond. A* **324**, 301–313. (doi:10.1098/rspa.1971.0141)
4. Derjaguin BV, Muller VM, Toporov YP. 1975 Effect of contact deformations on the adhesion of particles. *J. Colloid Interface Sci.* **53**, 314–326. (doi:10.1016/0021-9797(75)90018-1)
5. Tabor D. 1977 *Surface forces and surface interactions. Plenary and invited lectures*, pp. 3–14. New York, NY: Academic Press.
6. Maugis D. 1992 Adhesion of spheres: the JKR-DMT transition using a Dugdale model. *J. Colloid Interface Sci.* **150**, 243–269. (doi:10.1016/0021-9797(92)90285-T)
7. Muller V, Yushchenko V, Derjaguin B. 1980 On the influence of molecular forces on the deformation of an elastic sphere and its sticking to a rigid plane. *J. Colloid Interface Sci.* **77**, 91–101. (doi:10.1016/0021-9797(80)90419-1)
8. Greenwood J. 1997 Adhesion of elastic spheres. *Proc. R. Soc. Lond. A* **453**, 1277–1297. (doi:10.1098/rspa.1997.0070)
9. Fuller K, Tabor D. 1975 The effect of surface roughness on the adhesion of elastic solids. *Proc. R. Soc. Lond. A* **345**, 327–342. (doi:10.1098/rspa.1975.0138)
10. Persson B, Tosatti E. 2001 The effect of surface roughness on the adhesion of elastic solids. *J. Chem. Phys.* **115**, 5597–5610. (doi:10.1063/1.1398300)
11. Müser MH, Dapp WB, Bugnicourt R, Sainsot P, Lesaffre N, Lubrecht TA *et al.* 2017 Meeting the contact-mechanics challenge. *Tribol. Lett.* **65**, 118. (doi:10.1007/s11249-017-0900-2)
12. Medina S, Dini D. 2014 A numerical model for the deterministic analysis of adhesive rough contacts down to the nano-scale. *Int. J. Solids Struct.* **51**, 2620–2632. (doi:10.1016/j.ijsolstr.2014.03.033)
13. Solhjoo S, Vakis AI. 2016 Continuum mechanics at the atomic scale: Insights into non-adhesive contacts using molecular dynamics simulations. *J. Appl. Phys.* **120**, 215102. (doi:10.1063/1.4967795)
14. Wriggers P, Zavarise G. 2004 Computational contact mechanics. Encyclopedia of computational mechanics.

15. Rey V, Anciaux G, Molinari J-F. 2017 Normal adhesive contact on rough surfaces: efficient algorithm for FFT-based BEM resolution. *Comp. Mech.* **60**, 69–81. (doi:10.1007/s00466-017-1392-5)
16. Pastewka L, Robbins MO. 2014 Contact between rough surfaces and a criterion for macroscopic adhesion. *Proc. Natl Acad. Sci. USA* **111**, 3298–3303. (doi:10.1073/pnas.1320846111)
17. Afferrante L, Ciavarella M, Demelio G. 2015 Adhesive contact of the Weierstrass profile. *Proc. R. Soc. A* **471**, 20150248. (doi:10.1098/rspa.2015.0248)
18. Ciavarella M. 2015 Adhesive rough contacts near complete contact. *Int. J. Mech. Sci.* **104**, 104–111. (doi:10.1016/j.ijmecsci.2015.10.005)
19. Ciavarella M. 2018 A very simple estimate of adhesion of hard solids with rough surfaces based on a bearing area model. *Meccanica.* **53**, 241–250. (doi:10.1007/s11012-017-0701-6)
20. Pohrt R, Popov VL. 2015 Adhesive contact simulation of elastic solids using local mesh-dependent detachment criterion in boundary elements method. Facta Universitatis. *Ser. Mech. Eng.* **13**, 3–10.
21. Popov VL, Pohrt R, Li Q. 2017 Strength of adhesive contacts: influence of contact geometry and material gradients. *Friction.* **5**, 308–325. (doi:10.1007/s40544-017-0177-3)
22. Li Q, Pohrt R, Popov VL. 2019 Adhesive strength of contacts of rough spheres. *Front. Mech. Eng.* **5**, 7. (doi:10.3389/fmech.2019.00007)
23. Ghanbarzadeh A, Hassanpour A, Neville A. 2019 A numerical model for calculation of the restitution coefficient of elastic-perfectly plastic and adhesive bodies with rough surfaces. *Powder Technol.* **345**, 203–212. (doi:10.1016/j.powtec.2018.12.079)
24. Bazrafshan M, De Rooij M, Valefi M, Schipper D. 2017 Numerical method for the adhesive normal contact analysis based on a Dugdale approximation. *Tribol. Int.* **112**, 117–128. (doi:10.1016/j.triboint.2017.04.001)
25. Bazrafshan M, de Rooij M, Schipper D. 2018 On the role of adhesion and roughness in stick-slip transition at the contact of two bodies: A numerical study. *Tribol. Int.* **121**, 381–388. (doi:10.1016/j.triboint.2018.02.004)
26. Ciavarella M. 2019 Universal features in 'stickiness' criteria for soft adhesion with rough surfaces. *Tribol. Int.* **146**, 106031. (doi:10.1016/j.triboint.2019.106031)
27. Bhushan B, Majumdar A. 1992 Elastic-plastic contact model for bifractal surfaces. *Wear.* **153**, 53–64. (doi:10.1016/0043-1648(92)90260-F)
28. Persson B. 2014 On the fractal dimension of rough surfaces. *Tribol. Lett.* **54**, 99–106. (doi:10.1007/s11249-014-0313-4)
29. Müser MH. 2016 On the contact area of nominally flat hertzian contacts. *Tribol. Lett.* **64**, 14. (doi:10.1007/s11249-016-0750-3)
30. Pastewka L, Robbins MO. 2016 Contact area of rough spheres: Large scale simulations and simple scaling laws. *Appl. Phys. Lett.* **108**, 221601. (doi:10.1063/1.4950802)
31. Ciavarella M, Papangelo A. 2018 A modified form of Pastewka–Robbins criterion for adhesion. *J. Adhesion.* **94**, 155–165. (doi:10.1080/00218464.2017.1292139)
32. Persson BN, Scaraggi M. 2014 Theory of adhesion: role of surface roughness. *J. Chem. Phys.* **141**, 124701. (doi:10.1063/1.4895789)
33. Johnson K. 1995 The adhesion of two elastic bodies with slightly wavy surfaces. *Int. J. Solids Struct.* **32**, 423–430. (doi:10.1016/0020-7683(94)00111-9)